Journal of Energy Storage 50 (2022) 104674

Contents lists available at ScienceDirect

Journal of Energy Storage

journal homepage: www.elsevier.com/locate/est

Research papers

Evaluation of the energy storage capacity of Phase Change Material cement-lime mortars by using heat flux meters and ultrasonic pulse transmission

Cynthia Guardia *, Gonzalo Barluenga, Irene Palomar

Department of Architecture, University of Alcala, Madrid 28801, Spain

ARTICLE INFO

Keywords:
Phase Change Materials (PCM)
Energy storage
Cement-lime mortars
Ultrasonic testing
Heat flux

ABSTRACT

Materials with high energy storage capacity can enhance energy efficiency of buildings further than thermal insulation alone. The use of microencapsulated paraffin wax Phase Change Materials (PCM) in cement-lime mortars with cellulose fibres and lightweight aggregates (LWA) is a promising solution for this purpose. In this study, experimental techniques as flux heat meters and ultrasonic pulse transmission are used to evaluate the thermal performance and energy storage capacity of five cement-lime mortars with 20% of PCM, cellulose fibres and LWA (perlite) under different thermal conditions. A climatic chamber was used to simulate heating and cooling on one side of a sample plate of each mortar type, while the other side remained at lab conditions. Sample plates were instrumented with temperature-humidity sensors, heat flux meter plates and Ultrasonic (US) pulse transducers. US attenuation coefficient was used to identify the phase change PCM from solid to liquid and vice versa, during heating and cooling. The Heat flux difference between both sides of the plates was also measured during heating and cooling cycles. The specific enthalpy (energy storage capacity) of the mortars was calculated for heating and cooling cycles. Mixtures with LWA and PCM showed the best thermal performance achieving larger heat storage capacity than mortars with fibres or the combination of both LWA and fibres.

1. Introduction

The main characteristic of Phase Change Materials (PCM), their energy storage capacity at a certain temperature, can be useful to stabilise temperature and to storage and to release heat, enhancing energy efficiency of building enclosures [1–5]. Organic PCM, such as microencapsulated paraffin wax, are the most common PCM used in construction. They are very adaptable, commercial availability, and have good a price in comparison with other PCMs [6]. Some authors have already studied the thermal behaviour of PCM inside cement-based mortars with addition of other components (fibres and Lightweight aggregates - LWA), pointing out that PCM performance depends on the type of mixture where it was included [7–12].

Among the different characterization techniques (destructive and non-destructive) available for mortars [9,13–16], Ultrasonic pulse transmission (US) has become a powerful non-destructive tool for construction and building materials because it can be used both in the lab and in on-site applications [16–18]. With US, some mechanical properties related to porous materials' microstructure can be assessed. US accuracy is affected by ultrasonic frequency which is related to the wavelength. Besides ultrasonic pulse velocity, the raw US signal attenuation and the US attenuation coefficient can be used to evaluate energy absorption [16,17].

Although several techniques can be used for thermal evaluation of mortars [9,13,19], Differential Scanning Calorimetry (DSC) is the most commonly used for measuring the latent heat (enthalpy) when PCM is added [4,6,8,9]. The specific enthalpy can be obtained with DSC by applying a constant energy (K/min) on samples of a particular weight [20,21]. However, this test does not reflect the actual thermal performance of PCM mortars subjected to heating and cooling due to real climatic conditions [22,23]. There are several testing methods for evaluating PCM mortars thermal performance, simulating different climatic conditions with a climatic chamber or a thermal box [22,24–29] or through numerical simulations [8,23,30,31]. Heat transfer can be measured with heat flux meters while applying different climatic conditions [23,26,27,29,31,32,33]. Heat Flux meter plates can measure the heat that cross through the surface of a material over time [26,29].

This study is the last part of a research work that has been partially

* Corresponding author.
E-mail address: cynthia.guardia@edu.uah.es (C. Guardia).

https://doi.org/10.1016/j.est.2022.104674
Received 29 November 2021; Received in revised form 6 April 2022; Accepted 11 April 2022
Available online 21 April 2022

published [9,15,29]. The aim of this final part of study is to evaluate five different cement-lime mortars with PCM and different additions such as cellulose fibres and lightweight aggregates under different climatic conditions. Temperature and humidity sensors, Ultrasonic Pulse transducers (250 kHz) and heat flux meter plates were placed on mortar samples. Heating and cooling cycles inside a climatic chamber were applied on one side of the sample simulating different climatic conditions on one side, while the other remained at laboratory conditions, to evaluate the mortar thermal performance.

2. Experimental procedure

Five different cement-lime mortars were studied. Fig. 1 presents the decision- making criteria used to design mortar compositions: A reference cement-lime mortar was designed and afterwards modified with cellulose fibres (F), lightweight aggregates (LWA) and 20% of PCM (in volume of fresh mortar). The hardened mortars' properties were characterized and are summarized in Table 1. Afterwards, a climatic chamber was used to simulate different climatic conditions of heating and cooling processes and temperature, ultrasonic pulse propagation and heat flux evolution were evaluated.

2.1. Materials and mortars compositions

Cement-lime mortars were prepared using a white cement type BL II/B-L 32.5 N supplied by Cementos Portland Valderrivas and designated according to UNE-EN 197–1. An air lime class CL 90-S designated according to the European standard (UNE-EN 459–1) was used. The size of the siliceous sand aggregate added was 0-4 mm. A lightweight aggregate (LWA) was used, specifically an expanded perlite (L) with a particle size between 0 and 2 mm. Short cellulose fibres (F) of 1 mm length Fibracel® BC-1000 (Ø 20 μm), supplied by Omya Clariana S.L were also included. Finally, a microencapsulated paraffin wax Phase Change Material (PCM) was used. It was a microencapsulated paraffin wax Micronal® DS 5040× with a particle size ca. 50–300 μm, bulk density ca. 300–400 kg/m^3 and a melting point of ca. 23 ± 1 °C supplied by BASF Construction Chemicals España SL.

Table 1 shows the compositions of the five PCM cement-lime mortars analyzed.

A reference cement-lime mortar was designed (C). It was calculated a binder to aggregates ratio by volume of 1 (cement): 0.5 (lime): 4.5 (aggregate). Afterwards, 20% of Phase Change Material by fresh mortar volume was included (C_{20}). Then, dry cellulose fibres were added (1.5% of the total fresh mortar's volume), CF_{20}. Another mortar with a 50% replacement of siliceous aggregate with perlite was produced (CL_{20}). To get the same workability, plastic consistency, the water to binder ratio (w/b) was adjusted. The required values for façades rendering were taking into account (European standard UNE-EN 998–1). Finally, a mixture combining both fibres and perlite (CLF_{20}) was prepared.

The mixing process (less than 5 min) began with the mix of the dry components (30 s). Then water was added. In all cases it lasted until a homogenous mixture was obtained.

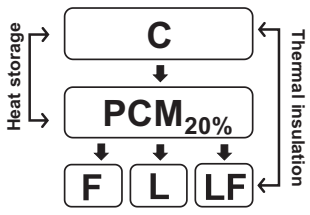

Fig. 1. Design schema of the PCM cement-lime mortars' composition under study.
C = Reference Mortar; PCM = Phase Change Material; F = cellulose fibres; L = Lightweight aggregates; LF = combination of Lightweight aggregates and cellulose fibres.

2.2. Experimental characterization techniques

Mortars were characterized both states, fresh and hardened. In order to measure the fresh mortar consistency and following the European standard UNE-EN 1015–3:200, the flow table test was carried out.

Several physical and mechanical hardened properties were characterized on 40x40x160 mm specimens (UNE-EN 1015–11). The equipment used to measure mortar strength was a Fully Automated, computer controlled, universal strength testing machine with a load cell of 20 T, manufactured by R.M.U Testing equipment. For thermal characterization, 210 mm × 210 mm and 24 ± 2 mm thick plate samples were manufactured. After 24 h the samples were removed from the mold. They were cured and tested at 28 days (21 ± 3 °C and 95 ± 5% RH).

The experimental set-up and testing techniques used for PCM mortars characterization have been described in a previous publication [9]. Geometrical density (D_g) of the sample plates was calculated considering the plates weight divided by the volume of each plate. Complying with UNE-EN 1015–10, open (accessible to water) porosity (OP) was calculated. Water vapour diffusion resistance factor (VD) was determined according to the European standard UNE-EN 1015–19. To calculate it, the wet-up method was used. Cylindrical samples of 35 mm diameter and 40 ± 2 mm thickness and 35 mm diameter with a saturated saline dissolution of 75%RH were used. Flexural and compressive strength were tested at 28 days on standard 40x40x160 mm prismatic specimens (European standard UNE-EN 1015–11).

Thermal conductivity of PCM mortars below and above PCM melting point (λ_S, λ_L) and phase change enthalpies (Differential Scanning Calorimetry) were calculated according to standard methods previously described [9,20,21]. Thermal conductivity was evaluated with a thermally insulated box. For the measurement, 210 × 210 × 24 ± 2 sample plates were used. Different temperature and humidity sensors were placed outside and inside the box and at the outer and inner and surface of the samples. Thermal conductivity (λ_S, λ_L) was calculated according to Fourier's Law [9,13,19].

A standardized PCM characterization procedure developed under the IEA Task 42- Annex 29 [21] was used to performed DSC measurements using a Mettler Toledo DSC1 device. The selected temperatures were 10 °C and 28 °C with isothermal segments of 5 min between each consecutive heating and cooling ramp, with a heating and cooling rate of 1 K/min.

The experimental set-up used for the laboratory simulation of climatic conditions is presented in Fig. 2. The climatic chamber used for the experimental set-up was a FDM C140SX (0–70 °C temperature and 10–98% of relative humidity ranges). The door of the chamber was replaced by a 50 mm expanded polystyrene (XPS) frame, covering the opening of the climatic chamber door completely, to produce a horizontal heat flux. The mortars plates (220 × 240 × 24 ± 2 mm) were placed in a central hole in the middle of the XPS frame (Fig. 2). Several temperatures (°C) and relative humidity (%) sensors were located outside and inside the climatic chamber, on both sides (in and out) of the mortar plates,

Two temperature values (15 °C and 30 °C) inside the climatic chamber, were considered to cross over the PCM melting point on the heating and cooling processes. The heating process began with an initial stable condition of 15 °C and 82% relative humidity (RH), switching afterwards the conditions to 30 °C and 33%RH. The cooling process consisted of an initial stable condition of 30 °C and 33%RH, changing to 15 °C and 82% RH. The laboratory conditions (outside the chamber) remained constant at 20 ± 1 °C and 60% RH. Relative Humidity inside the chamber was set to limit the water transport through sample plates.

Relative humidity (RH) was 80% and 33% respectively to minimize the effect of mass transfer on the energy transport between both sides of the sample plates. Laboratory conditions stayed constant at 20 ± 1 °C and 60 ± 5% RH.

Table 1
Compositions of PCM cement-lime mortars (components in kg for a batch of 1m^3 of mixture).

	Cement	CL 90-S	Sand(0–4)	Fibres	Perlite (A)	PCM	Water (B)	w/b	D_{dry} (kg/m^3)	D_{fresh} (kg/m^3)
C	348	55	1403	–	–	–	220	0.73	1400	2264
C_{20}	348	55	1403	–	–	84.6	200	0.68	1357	1937
CF_{20}	348	55	1403	0.66	–	84.6	240	0.78	1440	1885
CL_{20}	348	55	702	–	94	84.6	250	0.71	868	1562
CLF_{20}	348	55	702	0.59	94	84.6	380	0.79	–	1561

A) 50% of volume of the siliceous aggregate was replaced by perlite.
B) Liquid water added. Sand 0–4: Humidity 5.3% also taken into account.
C) D_{dry}: dry density of the components of the mixture. D_{fresh}: fresh density of the mixtures including the addition of water.

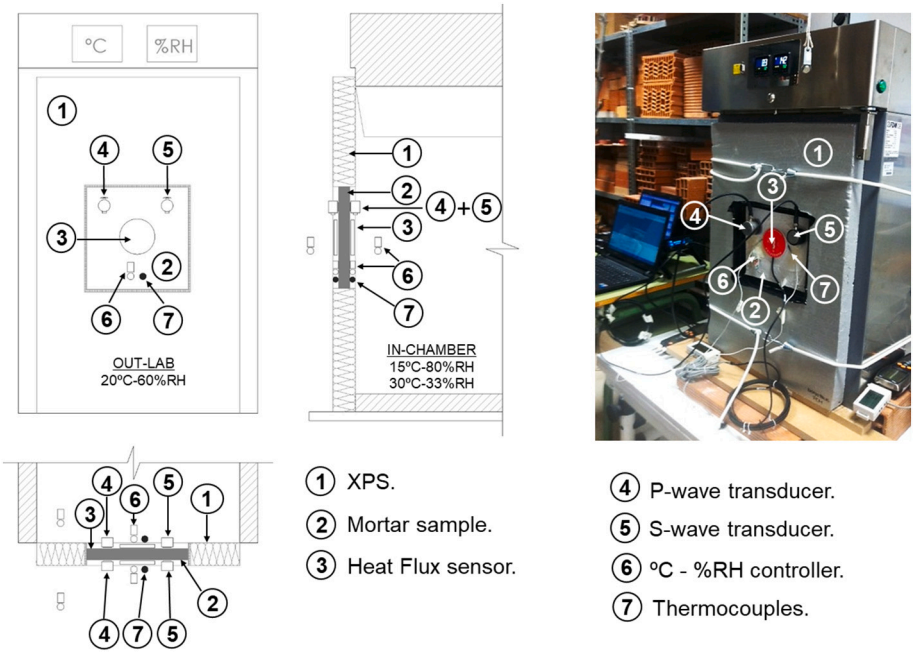

Fig. 2. Climatic Chamber set up for monitoring the samples at different temperature conditions.

Ultrasonic Pulse (US) 250 kHz P- and S-waves were also placed on the outer and inner surface of the plates (Fig. 2). The signal was computer recorded with an oscilloscope connected to the US device. Before placing the ultrasonic transducers on the material samples, the transmitter and receiver transducer were placed face to face to fix 0.0 transit time in order to calibrate the US device.

The amplitude (A_m) of the raw transmitted US signal in Volts trough the mortar samples was used to determine the attenuation coefficients of PCM mortars (AT_{PCM} in dB/mm), for liquid state PCM (AT_L), liquid-solid state PCM (AT_{L-S}) and solid state PCM (AT_S). AT_{PCM} was calculated using Eq. [16]:

$$AT_{PCM} = -(20/x)(log(A_m/A_T)) \quad (1)$$

where A_T is the amplitude (Volts) measured when the transmitter and receiver transmitter were placed face to face. Finally, x is the distance between transducers, which in this test corresponds to the plate thickness (24 ± 2 mm). It can be highlighted that the larger the attenuation coefficient AT_{PCM}, the higher the US energy absorbed by the sample.

Two heat flux meter plates (Hukseflux HFP01 with an uncertainty degree of ±3%) were placed in the centre of both sides of the sample plates to measure the heat flux (W/m^2) and a data logger (Hobo UX120) was used for the data acquisition during the test. The enthalpy of the sample plates was calculated according to Eqs. (2), (3) and (4):

$$\varnothing_T = \varnothing_{in} - \varnothing_{out} \quad (2)$$

$$\varnothing_Q = \int_{T0}^{Tf} \varnothing_T \, dT \quad (3)$$

$$h = [\varnothing_Q/(D_G \, e)] \cdot 1000 \quad (4)$$

where $\varnothing_T$ (in W/m^2) was the heat flux difference between inside ($\varnothing_{in}$) and outside ($\varnothing_{out}$) the climatic chamber. $\varnothing_Q$ (Jm^2) was the accumulated heat flux difference, considering the sample average temperature. Finally, h is the specific enthalpy of the mortar in MJ/g obtained from Eq. (4), where D_g (kg/m^3) is the geometrical density of the plates and e was the sample plate thickness (in mm). In all cases, a steady state at constant temperature (T) and relative humidity (RH) was set in the chamber, ensuring the same initial testing conditions for all mortars.

3. Experimental results

3.1. Hardened state PCM mortar properties

The five different cement-lime mortars properties (workability, physical, mechanical and thermal) are summarizes in Table 2. Some realtions between the compositions properties and parameters have been exposed and discussed in a previous work [9]. Plastic consistency was obtained for all the designed mortars.

Table 2 presents the geometric density (D_g), Open porosity (OP) and Water vapour diffusion resistance factor (VD) of the mortar plates

Table 2
Workability, physical, mechanical, and thermal properties of PCM cement-lime mortars.

	Workability	Physical properties			Mechanical properties		Thermal properties	
	Consistency mm	D_g kg/m^3	OP %	VD -	CS MPa	FS MPa	λ_S W/mK	λ_L W/mK
C	178	1985	19.56	4.13	14.33	3.36	0.23	0.21
C_{20}	166	1607	17.72	4.29	7.17	2.40	0.20	0.28
CF_{20}	170	1747	16.77	3.47	5.83	2.20	0.30	0.23
CL_{20}	170	1287	23.33	3.62	6.0	1.79	0.29	0.18
CLF_{20}	170	1196	23.09	3.26	5.33	2.16	0.23	0.15

prepared for this study. As expected, the reference mortar without PCM (C) presented the highest D_g (1985 kg/m^3), while CLF_{20} showed the lowest, 1196 kg/m^3. CF_{20} showed the lowest Open porosity (OP) value (16.77%) and CLF_{20} the highest one (23.33%). Water vapour diffusion resistance factor (VD) varied between 3.26 (CLF_{20}) and 4.29 (C_{20}).

Table 2 also reports the compressive (CS) and flexural (FS) strength results. The lowest CS value was obtained for CLF_{20} (5.33 MPa), while C showed the highest (14.33 MPa).

Accordingly, to a CS-III grade rendering mortar, according to the European standard UNE-EN 998–1. all the mixtures reached the target minimum compressive strength value of 3.5 MPa. Flexural strength results varied between 1.79 MPa for CL_{20} and 3.36 MPa for C.

Table 2 also shows thermal conductivity of PCM mortars when PCM was in a solid (λ_S) or liquid (λ_L) states, calculated when samples reached a thermal steady state below and above PCM melting point (23 °C). C_{20} presents the lowest λ_S value (0.20 W/mK) while CF_{20} presents the highest one (0.30 W/mK). In can be observed that λ_L varied between 0.15 W/mK (CLF_{20}) and 0.28 W/mK (C_{20}).

3.2. Ultrasonic identification of PCM phase change

Fig. 3 shows the paraffin wax PCM solidification process inside a PCM microcapsule during a cooling cycle of a mortar sample with 20% of PCM (C_{20}) [9] and the associated raw US signal (250 kHz p- and s-wave). Initially, the liquid paraffin filled the whole capsule as the temperature was above the PCM melting point ($T > 23$ °C, PCM_L). When the temperature began to drop, the phase change of the paraffin begun (releasing energy), produced a mixed liquid-solid phase ($T \leq 23$ °C, $PCM_{L\text{-}S}$). Finally, as the temperature dropped under 23 °C (PCM_S), all the paraffin changed into a solid phase.

Ultrasonic (US) monitoring was applied on the samples in order to use this non-destructive testing technique to identify the phase change process. In the different stages of the process the same transmission time was recorded for the voltage peak (18 μs), while the voltage amplitude of the wave varied depending on the PCM. When PCM was in a liquid phase, as the average temperature of the sample was above 23 °C, the voltage peak reached 10 V. The decrease of temperature of the sample reaching on one side of the plate 23 °C, corresponding with the PCM phase change, the received US wave voltage peak increased up to 35 V. Finally, as the temperature decreased below 23 °C, all the PCM reached a solid state and the voltage peak was 70 V, corresponding to the lowest wave attenuation. Accordingly, PCM in a liquid phase produced larger transmitted US wave attenuation than the solid phase and the phase change can be monitored using this non-destructive technique.

3.3. US wave attenuation coefficients of PCM mortars

Table 3 presents the attenuation coefficient of PCM mortars at a liquid (AT_L), liquid-solid ($AT_{L—S}$) and solid phase (AT_S), obtained using Eq. (1). As expected, the mixture without PCM (C) showed a linear trend close to 1 dB/mm), decreasing slightly with temperature (AT_L was 0.99 dB/mm while AT_S was 0.86 dB/mm), probably due to changes in humidity inside the pore microstructure of the sample.

Samples with PCM showed larger variations of AT_{PCM} (attenuation coefficients of PCM mortars), related not only on PCM phases but also on the mortar composition. When PCM was in liquid state ($T > 23$ °C), AT_L varied between 1.33 dB/mm (CL_{20}) and 0.57 dB/mm (CF_{20}). As temperature decreased ($T \geq 23$ °C), phase change began and AT_{PCM} decreased (US absorption decreased). CL_{20} showed the highest $AT_{L\text{-}S}$ value (1.13 dB/mm) while C_{20} presented the lowest one (0.30 dB/mm). When temperature decreased below PCM melting point, AT_S decreased regarding $AT_{L—S}$. CL_{20} presented the highest value (1.05 dB/mm) and

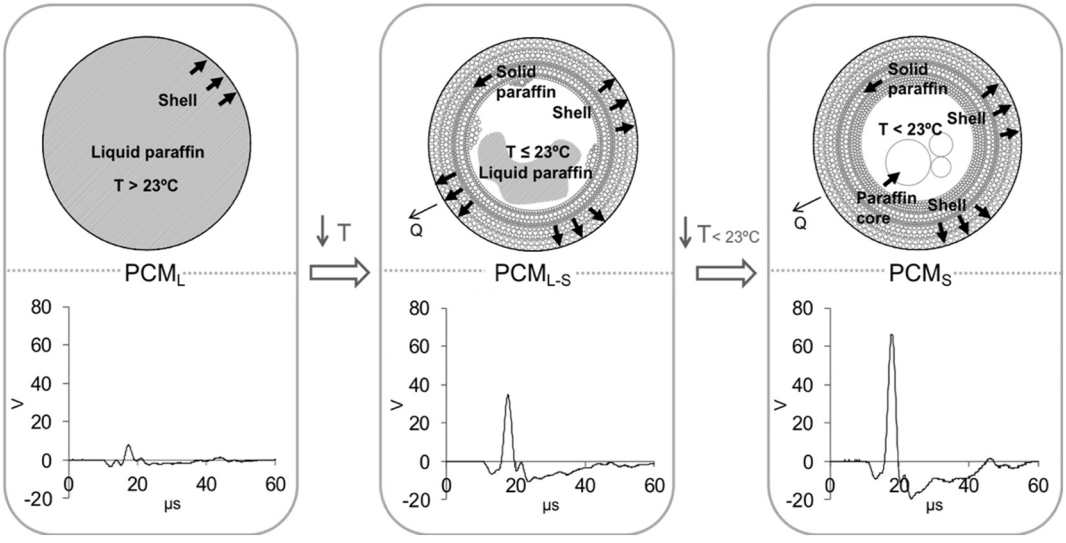

Fig. 3. PCM solidification process inside a PCM microcapsule [9] and the associated raw US signal (250 kHz p- and s-wave) during a cooling cycle of a mortar sample with 20% of PCM (C_{20}).

Table 3
Attenuation coefficient AT_{PCM} (attenuation coefficients of PCM mortars in dB/mm) of 250 kHz US transmission of PCM mortars at different PCM phases.

	C	C_{20}	CF_{20}	CL_{20}	CLF_{20}
AT_L (Liquid) ($T > 23$ °C)	0.99	0.84	0.57	1.33	1.29
$AT_{L\text{-}S}$ (Liquid-solid) ($T \leq 23$ °C)	0.92	0.30	0.46	1.13	1.02
AT_S (Solid) ($T < 23$ °C)	0.86	0.05	0.42	1.05	0.96

AT_L Liquid: attenuation coefficients of the mortar when PCM is in liquid state ($T > 23$ °C).
$AT_{L\text{-}S}$ (Liquid-solid): attenuation coefficients of the mortar when PCM is changing from liquid to solid state ($T \leq 23$ °C).
AT_S (Solid): attenuation coefficients of the mortar when PCM is in solid state ($T < 23$ °C).

C_{20} the lowest (0.05 dB/mm).

3.4. DSC enthalpy of PCM mortars

Fig. 4 presents the specific enthalpy of the five PCM mortars during heating and cooling cycles measured with Differential Scanning Calorimetry (DSC). The temperature interval was defined between 10 °C and 28 °C. The enthalpy of reference mixture C (mixture without PCM) presented a linear dependence of temperature, as expected. The addition of 20% of PCM exhibited slight differences between heating and cooling cycles. However, in both cases an inflection point corresponding to the PCM melting point was observed, located at 23 °C for heating cycles and at 22 °C for cooling cycles [9].

Mortar composition also affected the specific enthalpy values. Reference mortar C (without PCM) presented the lowest specific enthalpy value (15 J/g) for 28 °C, while PCM mortars with cellulose fibres (CF_{20} and CLF_{20}) increased enthalpy up to 20 J/g, C_{20} reached 21.5 J/g and samples with LWA (CL_{20}) went up to 25 J/g. As concluded in a preciously work [9], the enthalpy of the mixtures depends both on PCM and on the other components added to mixtures.

3.5. Temperature and heat flux during heating and cooling cycles

Fig. 5 plots the average temperature and heat flux difference between inner and outer sides of mortar samples $\varnothing_T$ (in W/m^2), during heating and cooling cycles simulated with a climatic chamber. In all

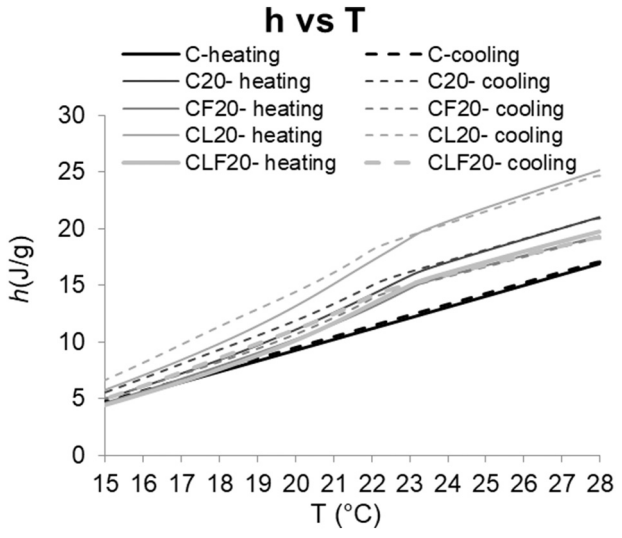

Fig. 4. Cement-lime mortars enthalpy measured in DSC during heating and cooling cycles.

cases, the same test procedure was followed to ensure a solid or liquid initial PCM steady state, at the beginning of each cycle respectively. For heating cycles (PCM melting), the climatic chamber was set at 15 °C (time = 0 s). After the steady state was reached, temperature inside the chamber was increased up to 30 °C. For the cooling cycle (PCM solidification), the climatic chamber was set at 30 °C until the steady state was reached and temperature was reduced to 15 °C afterwards.

During heating cycles (Fig. 5a), the reference mixture without PCM (C) presented an average temperature lower than PCM mortars. Mortars C_{20}, CL_{20} and CLF_{20} reached PCM melting point (23 °C) between 1800s and 2400 s, while CF_{20} delayed up to 3000 s. This delay can be related to the mortar density recorded in Table 2, where C was the mixture with the highest D_g (2376 kg/m^3). As expected, the higher D_g, the longer took the material to increase its temperature. The steady state regime was achieved at 27 °C, although C and CF_{20} showed an average temperature 0.5 °C lower than the other mixtures.

Cooling cycles showed the influence of LWA on the thermal process (Fig. 5b). Temperature evolution was similar for all samples after reaching the solidification temperature of 21 °C [9], being CLF_{20} the mixture that took more time to achieve it. Thermal insulation capacity of LWA was behind this difference. At the end of the test, Mortar without PCM (C_{20}) recorded the lowest temperature (17 °C), 2 °C below CL_{20}, which was the mixture with the highest final average temperature (19 °C).

Fig. 5c and d relate the heat flux difference $\varnothing_T$ (in W/m^2) to the average temperature (plotted in Fig. 5a and b). $\varnothing_T$ (in W/m^2) corresponded to the heat stored and released by the sample at each average temperature during the heating and cooling cycle, respectively. The main pattern followed in both processes had an initial increase of the heat flux until maximum peak was reached and afterwards a decrease until steady state was reached and $\varnothing_T$ was 0 W/m^2.

During heating cycles (Fig. 5d), reference mortar (C) showed the highest peak of heat flux (151.41 W/m^2 at 20 °C), while CLF_{20} presented the lowest (102.95 W/m^2 at 23 °C). It can be assumed that the largest D_g was behind this difference. It can be observed that mortar C showed a different behaviour than mixtures with PCM. PCM mortars exhibited a plateau around PCM melting temperature (between 22 °C and 24 °C) that can be assumed to correspond to the latent heat required for PCM melting, while reference mortar did not show this plateau. In this case, only sensible heat affected the mixture.

During cooling cycles (Fig. 5d), C was again the mixture with the highest maximum peak (130.00 W/m^2 at 23.5 °C) and CLF_{20} showed the lowest peak (110.05 W/m^2 at 25.5 °C). In this case, PCM mortars showed again a constant heat flux value at solidification temperature (23 °C- 21 °C [9]) corresponding to the phase change of PCM (latent heat). Afterwards, as it occurred in the heating process, heat flux decreased until a steady state was reached ($\varnothing_T$ was 0 W/m^2.).

4. Analysis and discussion

The experimental results pointed out that the thermal behaviour of mortars with PCM depended not only on PCM volumetric fraction but also on mixture composition. The US attenuation coefficient for each mixture at different PCM states is analyzed and the mortar specific enthalpy (capacity of mortars to absorb or release energy) at different temperature conditions is also discussed.

4.1. Influence of mortar microstructure and PCM state on US attenuation coefficient

Fig. 6 presents the experimental results of AT_{PCM} at different PCM states showed in Table 3. PCM mortar without LWA or fibres (C_{20}) showed the largest AT_{PCM} variation. The incorporation of LWA increased AT_{PCM} for all the PCM states considered (liquid, liquid-solid and solid) above 1 dB/mm. because lightweight aggregates absorbed US energy, due to its large porosity [15], which produced mortars with larger OP

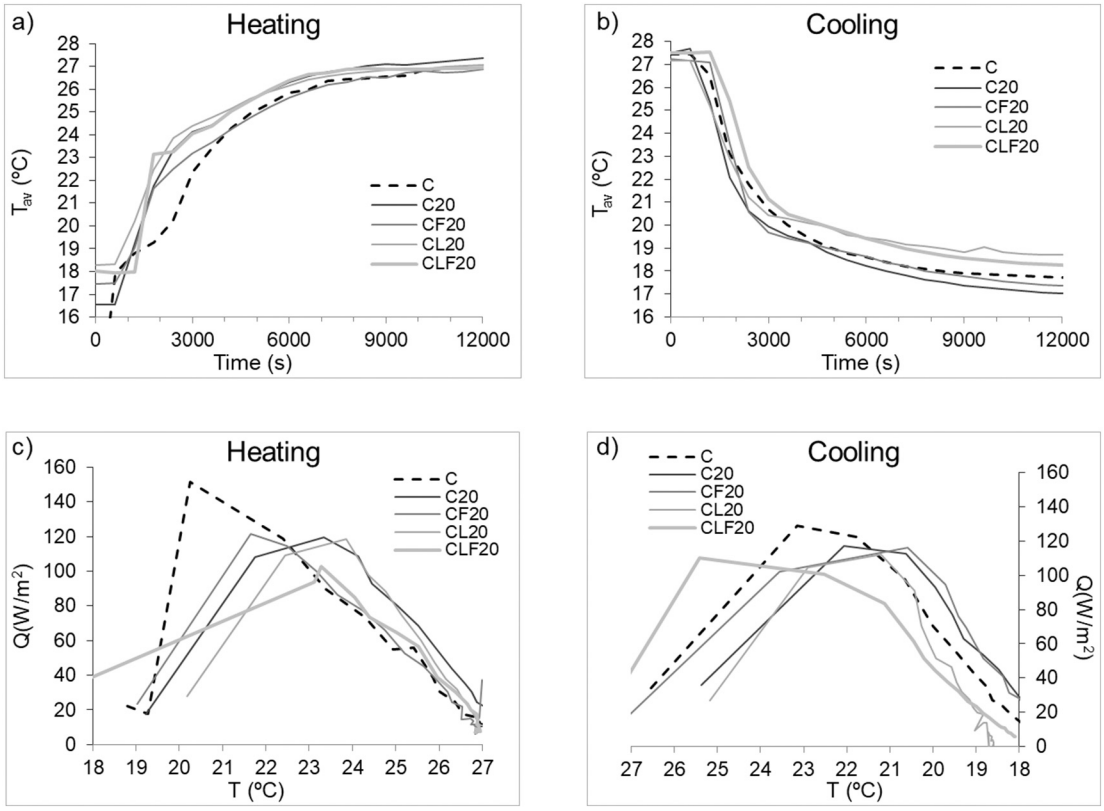

Fig. 5. Sample average temperature (T_{av}) and Heat flux (Q) difference between inner and outer sample sides during heating at cooling cycles measured on mortar samples.

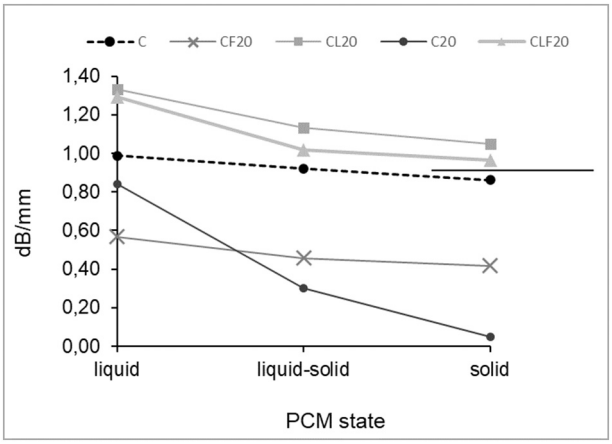

Fig. 6. Attenuation coefficient at different PCM states.

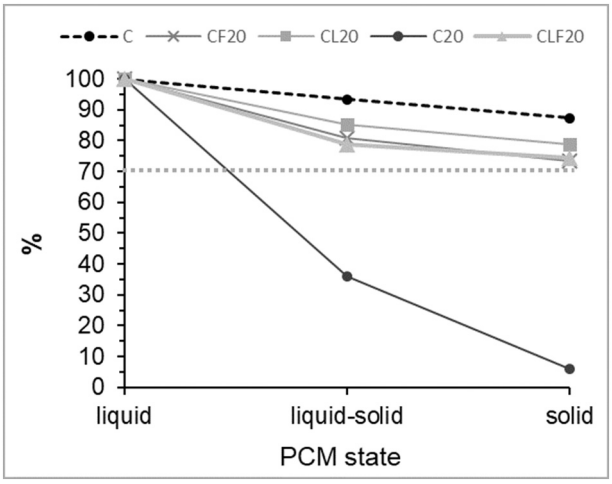

Fig. 7. Relative attenuation values (%) related to PCM states.

and lower D_G (Table 2). Accordingly, it can be said that the lower the density of the mixture, the higher is the attenuation coefficient.

The relative values of AT_{PCM} are plotted in Fig. 7, where 100% corresponded to AT_L in each case. The decrease of AT_{PCM} was related to the liquid to solid transition and reached 30% in all cases but C_{20}, where the reduction reached 95%. As expected, the reference mortar without PCM (C) showed a slight decrease that can be related to de water content of the sample (it must be considered that water is also a PCM). Accordingly, US attenuation coefficient AT_{PCM} can be used as an indirect measurement to identify PCM phase change inside a PCM cement-lime mortar.

4.2. Mortar specific enthalpy assessment of PCM mortars during heating and cooling cycles

Fig. 8 presents the specific enthalpy (h) calculated using Eqs. (2)–(4) during heating (heat storage) and cooling (heat release) cycles. During the heating cycle, from 18 °C and 27 °C, *h* varied between 11.4 MJ/g (CF_{20}) and 15.82 MJ/g (CL_{20}). CLF_{20} and C_{20} showed the same enthalpy value, 15 MJ/g. On the other hand, during the cooling cycle, from 18 °C and 27 °C, *h* varied between 15.96 MJ/g (CL_{20}) and 10.14 MJ/g (CF_{20}). CLF_{20} showed an enthalpy value at 18 °C of 15.9 MJ/g while C_{20} recorded 13.44 MJ/g.

As expected, the reference mortar without PCM (C) showed a linear

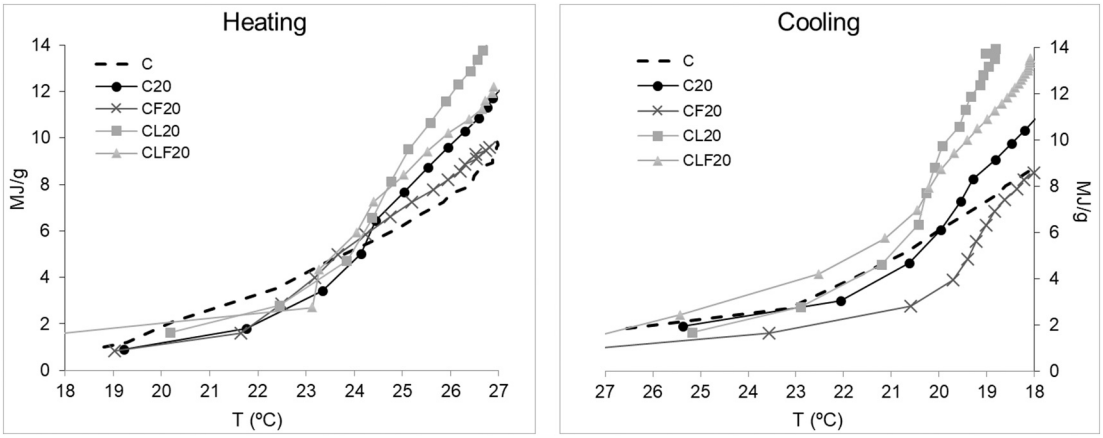

Fig. 8. PCM cement-lime mortars enthalpy during heating and cooling cycles.

trend with temperature, which agrees with the results obtained with the Differential Scanning Calorimetry (Fig. 4). On the other hand, PCM mortars showed a variation on the curve slope corresponding to the PCM melting point observed in DSC tests: 22–24.5 °C for heating and 22–19 °C for cooling (Fig. 4) [9].

As shown in Fig. 8a, the energy necessary to produce PCM phase change in the temperature interval during heating from 22 °C to 24.5 °C was 4.5 MJ/g for mortars CF_{20}, C_{20} and CLF_{20} required 5 MJ/g and CL_{20} needed up to 5.5 MJ/g. Consequently, CL_{20} was the mixture with higher heat storage capacity. During the cooling cycle, the specific enthalpy necessary for PCM solidification through the temperature interval 22–19 °C was 4.5 MJ/g for CF_{20}, 6 MJ/g for C_{20}, 7.5 MJ/g for CLF_{20} and 9.5 MJ/g for CL_{20}.

Summarising, PCM mortar with LWA (CL_{20}) presented the best thermal performance due to its largest heat storage capacity (largest enthalpy) and thermal insulation (lowest conductivity). These results correspond with the results obtained with the DSC measurements where CL_{20} was also the mixture that presented the best specific enthalpy.

5. Conclusions

An experimental study to assess the thermal performance and energy storage capacity of cement-lime mortars with the addition of 20% of PCM, a perlite lightweight aggregate (LWA) and cellulose fibres during heating and cooling cycles was presented. A physical, thermal, and mechanical characterization was carried out on hardened mortar samples. A laboratory simulation of heating and cooling cycles using a climatic chamber was conducted on mortar sample plates. Ultrasonic pulses (US) were used to evaluate the heating-cooling processes and heat flux and temperature was measured at both sides of the sample plate. The main conclusions of this study were:

- The addition of 20% of PCM increased the energy storage capacity of cement-lime mortars due to the latent heat required for phase change. The incorporation of LWA and fibres also modified mortar's properties, included thermal conductivity and enthalpy measured with Differential Scanning Calorimetry (DSC).
- Ultrasonic pulse attenuation was used to identify the phase change of PCM inside the mortar during heating and cooling cycles. PCM melting reduced US Attenuation coefficient.
- The specific enthalpy of PCM mortars was evaluated measuring temperature and heat flux on both sides of a mortar plate subjected to heating and cooling using a climatic chamber. The experimental results fully agree with DSC test results.
- PCM cement-lime mortar with LWA (CL_{20}) showed the best thermal performance during heating and cooling cycles due to its higher specific enthalpy and its lower thermal conductivity.

CRediT authorship contribution statement

Cynthia Guardia: Conceptualization, Methodology, Formal analysis, Data curation, Investigation, Writing – original draft, Writing – review & editing. **Gonzalo Barluenga:** Conceptualization, Methodology, Formal analysis, Investigation, Writing – original draft, Writing – review & editing, Supervision, Project administration. **Irene Palomar:** Conceptualization, Methodology, Investigation, Writing – review & editing, Project administration, Funding acquisition.

Declaration of competing interest

The authors declared that there is no conflict of interest.

Acknowledgements

Some of the components were supplied by Omya Clariana S.L., BASF Construction Chemicals España S.L, and Cementos Portland Valderrivas. Financial support for this research was provided by the Research Program for the Promotion of Young Researchers, co-funded by Comunidad de Madrid and the University of Alcala (Spain), as part of the project IndoorComfort (CM/JIN/2019-46).

References

[1] A. Kasaeian, L. Bahrami, F. Pourfayaz, E. Khodabandeh, W.M. Yan, Experimental studies on the applications of PCMs and nano-PCMs in buildings: a critical review, Energy Build. 154 (2017) 96–112, https://doi.org/10.1016/j.enbuild.2017.08.037.

[2] L.F. Cabeza, C. Barreneche, A. Castell, A. de Garcia, et al., Materials used as PCM in thermal energy storage in building: a review, Renew. Sust. Energ. Rev. 15 (2011) 1675–1695, https://doi.org/10.1016/j.rser.2010.11.018.

[3] D. Zhou, C.Y. Zhao, Y. Tian, Review on thermal energy storage with phase change materials (PCMs) in building applications, Appl. Energy 92 (2012) 593–605, https://doi.org/10.1016/j.apenergy.2011.08.025.

[4] E. Günther, S. Hiebler, H. Mehling, R. Redlich, Enthalpy of phase change materials as a function of temperature: required accuracy and suitable measurement methods, Int. J. Thermophys. 30 (2009) 1257–1269, https://doi.org/10.1007/s10765-009-0641-z.

[5] R.K. Sharma, P. Ganesan, V.V. Tyagi, H.S.C. Metselaar, S.C. Sandaran, Developments in organic solid–liquid phase change materials and their applications in thermal energy storage, Energy Convers. Manag. 95 (2015) 193–228, https://doi.org/10.1016/j.enconman.2015.01.084.

[6] S. Drissi, A. Eddhahak, S. Caré, J. Neji, Thermal analysis by DSC of phase change materials, study of the damage effect, J. Build. Eng. 1 (2015) 13–19, https://doi.org/10.1016/j.jobe.2015.01.001.

[7] Rao V. Venkateswara, R. Parameshwaran, Ram V. Vinayaka, PCM-mortar based construction materials for energy efficient buildings: a review on research trends, Energy Build. 158 (2018) 95–122, https://doi.org/10.1016/j.enbuild.2017.09.098.

[8] C. Mankel, A. Caggiano, N. Ukrainczyk, E. Koenders, Thermal energy storage characterization of cement-based systems containing microencapsulated-PCMs, Constr. Build. Mater. 199 (2019) 307–320, https://doi.org/10.1016/j.conbuildmat.2018.11.195.

[9] C. Guardia, G. Barluenga, I. Palomar, G. Diarce, Thermal enhanced cement-lime mortars with phase change materials (PCM), lightweight aggregate and cellulose fibers, Constr. Build. Mater. 221 (2019) 586–594, https://doi.org/10.1016/j.conbuildmat.2019.06.098.
[10] A. Jayalath, Nicolas R. San, M. Sofi, R. Shanks, T. Ngo, L. Aye, P. Mendis, Properties of cementitious mortar and concrete containing micro-capsulated phase change materials, Constr. Build. Mater. 120 (2016) 408–417, https://doi.org/10.1016/j.conbuildmat.2016.05.116.
[11] S. Lucas, V.M. Ferreira, J.L. Barroso de Aguiar, Latent heat storage in PCM containing mortars—study of microstructural modifications, Energy Build. 66 (2013) 724–731, https://doi.org/10.1016/j.enbuild.2013.07.060.
[12] S. Cunha, M. Lima, J.B. Aguiar, Influence of adding phase change materials on the physical and mechanical properties of cement mortars, Constr. Build. Mater. 127 (2016) 1–10, https://doi.org/10.1016/j.conbuildmat.2016.09.119.
[13] I. Palomar, G. Barluenga, J. Puentes, Lime–cement mortars for coating with improved thermal and acoustic performance, Constr. Build. Mater. 75 (2015) 306–314, https://doi.org/10.1016/j.conbuildmat.2014.11.012.
[14] G. Barluenga, J. Puentes, I. Palomar, C. Guardia, Methodology for monitoring cement based materials at early age combining NDT techniques, Constr. Build. Mater. 193 (2018) 373–383, https://doi.org/10.1016/j.conbuildmat.2018.10.205.
[15] C. Guardia, D.S. Schicchi, A. Caggiano, G. Barluenga, E. Koenders, On the capillary water absorption of cement-lime mortars containing phase change materials: experiments and simulations, Build. Simul. 13 (2020) 19–31, https://doi.org/10.1007/s12273-019-0556-y.
[16] I. Palomar, G. Barluenga, Assessment of lime-cement mortar microstructure and properties by P- and S- ultrasonic waves, Constr. Build. Mater. 139 (2017) 334–341, https://doi.org/10.1016/j.conbuildmat.2017.02.083.
[17] T.P. Philippidis, D.G. Aggelis, Experimental study of wave dispersion and attenuation in concrete, Ultrasonics 43 (2005) 584–595, https://doi.org/10.1016/j.ultras.2004.12.001.
[18] Z. Lafhaj, M. Goueygou, A. Djerbi, M. Kaczmarek, Correlation between porosity, permeability and ultrasonic parameters of mortar with variable water/cement ratio and water content, Cem. Concr. Res. 36 (4) (2006) 625–633, https://doi.org/10.1016/j.cemconres.2005.11.009.
[19] S. Herrero, P. Mayor, F. Hernández-Olivares, Influence of proportion and particle size gradation of rubber from end-of-life tires on mechanical, thermal and acoustic properties of plaster–rubber mortars, Mater. Des. 47 (2013) 633–642, https://doi.org/10.1016/j.matdes.2012.12.063.
[20] A. Ristić, S. Furbo, C. Moser, H. Schranzhofer, et al., IEA SHC task 42 / ECES annex 29 WG A1: engineering and processing of PCMs, TCMs and sorption materials, Energy Procedia 91 (2016) 207–217, https://doi.org/10.1016/j.egypro.2016.06.205.
[21] S. Gschwander, T. Haussmann, G. Hagelstein, A. Sole, L.F. Cabeza, G. Diarce, et al., Standardization of PCM characterization via DSC, in: 13th International Conference on Energy Storage, 2015, pp. 19–21.
[22] S. Cunha, P. Leite, J. Aguiar, Characterization of innovative mortars with direct incorporation of phase change materials, J. Energy Storage 30 (2020), 101439, https://doi.org/10.1016/j.est.2020.101439.
[23] T. Pirasaci, Investigation of phase state and heat storage form of the phase change material (PCM) layer integrated into the exterior walls of the residential-apartment during heating season, Energy 207 (2020), 118176, https://doi.org/10.1016/j.energy.2020.118176.
[24] A. Gounni, M. El Alami, The optimal allocation of the PCM within a composite wall for surface temperature and heat flux reduction: an experimental approach, Appl. Therm. Eng. 127 (2017) 1488–1494, https://doi.org/10.1016/j.applthermaleng.2017.08.168.
[25] S.S. Lucas, J.L. Barroso de Aguiar, Evaluation of latent heat storage in mortars containing microencapsulated paraffin waxes – a selection of optimal composition and binders, Heat Mass Transf. 55 (2019) 2429–2435, https://doi.org/10.1007/s00231-019-02594-1.
[26] I. Palomar, G. Barluenga, R.J. Ball, M. Lawrence, Laboratory characterization of brick walls rendered with a previous lime-cement mortar, J. Build. Eng. 23 (2019) 241–249, https://doi.org/10.1016/j.jobe.2019.02.001.
[27] R.J. Khan, Z.H. Bhuiyan, D.H. Ahmed, Investigation of heat transfer of a building wall in the presence of phase change material (PCM), Energy Built Environ. 1 (2) (2020) 199–206, https://doi.org/10.1016/j.enbenv.2020.01.002.
[28] A. Sarcinella, J.L.B. De Aguiar, M. Lettieri, S. Cunha, M. Frigione, Thermal performance of mortars based on different binders and containing a novel sustainable phase change material (PCM), Materials 13 (2020) 2055, https://doi.org/10.3390/ma13092055.
[29] C. Guardia, G. Barluenga, I. Palomar, PCM cement-lime mortars for enhanced energy efficiency of multilayered building enclosures under different climatic conditions, Materials 13 (2020) 4043, https://doi.org/10.3390/ma13184043.
[30] S. Moreno, J.F. Hinojosa, I. Hernández-López, J. Xaman, Numerical and experimental study of heat transfer in a cubic cavity with a PCM in a vertical heated wall, Appl. Therm. Eng. 178 (2020), 115647, https://doi.org/10.1016/j.applthermaleng.2020.115647.
[31] V.D. Fachinotti, F. Bre, C. Mankel, E.A.B. Koenders, A. Caggiano, Optimization of multilayered walls for building envelopes including PCM-based composites, Materials 13 (2020) 2787, https://doi.org/10.3390/ma13122787.
[32] Valentina Sierra, Farid Chejne, Energy saving evaluation of microencapsulated phase change materials embedded in building systems, J. Energy Storage. ISSN: 2352-152X 49 (2022) 104102, https://doi.org/10.1016/j.est.2022.104102.
[33] F. Rebelo, A. Figueiredo, R. Vicente, V.M. Ferreira, Study of a thermally enhanced mortar incorporating phase change materials for overheating reduction in buildings, J. Energy Storage. ISSN: 2352-152X 46 (2022) 103876, https://doi.org/10.1016/j.est.2021.103876.